

Article

Covalent Si–H Bonds in the Zintl Phase Hydride CaSiH_{1+x} ($x \leq 1/3$)[†]

Henry Auer^{1,*}, Fangshun Yang¹, Helen Y. Playford², Thomas C. Hansen³, Alexandra Franz⁴
and Holger Kohlmann^{1,*}¹ Institute of Inorganic Chemistry, Leipzig University, Johannisallee 29, 04103 Leipzig, Germany² The ISIS Facility, STFC Rutherford Appleton Laboratory, Chilton, Didcot, Oxfordshire OX11 0QX, UK³ Institut Laue-Langevin, 71 avenue des Martyrs, 38000 Grenoble, France⁴ Helmholtz-Zentrum Berlin, Hahn-Meitner-Platz 1, 14109 Berlin, Germany* Correspondence: henry.auer@gmx.de (H.A.); holger.kohlmann@uni-leipzig.de (H.K.);
Tel.: +49-341-9736201 (H.K.)

† Dedicated to Prof. Dr. Joachim Sieler on the Occasion of his 80th Birthday.

Received: 26 June 2019; Accepted: 7 August 2019; Published: 21 August 2019



Abstract: The crystal structure of the Zintl phase hydride $\text{CaSiH}_{\approx 4/3}$ was discussed controversially, especially with respect to the nature of the silicon-hydrogen interaction. We have applied X-ray and neutron powder diffraction as well as total neutron scattering on a deuterated sample, $\text{CaSiD}_{1.1}$. Rietveld refinement ($\text{CaSiD}_{1.1}$, $Pnma$, $a = 14.579(4)$ Å, $b = 3.8119(4)$ Å, $c = 11.209(2)$ Å) and an analysis of the neutron pair distribution function show a silicon-deuterium bond length of 1.53 Å. The Si–H bond may thus be categorized as covalent and the main structural features described by a limiting ionic formula $\text{Ca}^{2+}\text{H}^-(\text{Si}^-)_{2/3}(\text{SiH}^-)_{1/3}$. Hydrogen atoms decorating the ribbon-like silicon polyanion made of three connected zigzag chains are under-occupied, resulting in a composition $\text{CaSiH}_{1.1}$. Hydrogen-poor Zintl phase hydrides $\text{CaSiH}_{<1}$ with hydride ions in Ca_4 tetrahedra only were found in an in situ neutron diffraction experiment at elevated temperature. Hydrogen (deuterium) uptake and release in CaSiD_x ($0.05 \leq x \leq 0.17$) is a very fast process and takes less than 1 min to complete, which is of importance for possible hydrogen storage applications.

Keywords: Zintl phase; Zintl phase hydride; metal hydride; neutron diffraction; Rietveld refinement; pair distribution function; polyanions; hydrogen storage; silicon; in situ

1. Introduction

During the last twenty years, a new class of compounds has been developed: Hydrides of Zintl phases exhibiting hydrogen atoms coordinated to a polyanion. The first examples were $\text{Ae}(\text{TrH})_2$ and $\text{Ae}(\text{TrH})\text{Tt}$, $\text{Ae} = \text{Ca–Ba}$, $\text{Tr} = \text{Al–In}$, $\text{Tt} = \text{Si–Sn}$ [1–8]. These phases show a puckered honeycomb-like structure of Tr or Tr and Tt atoms. Hydrogen is bound to the group 13 element. The interaction is clearly covalent, as indicated by a short bond length and neutron vibrational spectroscopy [4,6–8]. Such pseudo-molecular moieties are referred to as polyanionic hydrides [9]. In contrast, there are LnGaH_{1+x} ($\text{Ln} = \text{Nd}$ [10,11], Gd [12], $x < 1$) phases that show a pronounced homogeneity range for the hydrogen incorporation [11]. One hydrogen per formula unit occupies a tetrahedral Ln_4 void (interstitial hydride). The remaining hydrogen atoms are located in trigonal-bipyramidal Ln_3Ga_2 voids. The Ga–H distance is rather long (≈ 2 Å). The same structure motif was recently found for $\text{LaGa}_2\text{H}_{0.71(2)}$ [13] as well. The bonding situation is comparable to classical metallic hydrides like $\text{PdH}_{0.7}$ rather than to covalent ones.

The existence of polyanionic hydrides with a covalent element-hydrogen bond (next to an element–element bond) of group 14 elements was long unclear. The Zintl phase hydride $\text{CaSiH}_{\approx 4/3}$

was the first example of this type of compound with a silicon-backbone and a silicon-hydrogen contact [14–17]. The system CaSi-H_2 also gathered interest as a potential hydrogen storage material with 1.9 wt % hydrogen capacity and good reversibility at mild conditions (473–573 K) [14,15].

Considering the idealized chemical formula $\text{CaSiH}_{4/3}$, the material can be understood according to the rules of hydrogen incorporation in Zintl phases [9]. There are two types of hydrogen atoms present. One is incorporated as hydride ion in sheets of edge sharing calcium tetrahedra, $(\text{HCa}_{4/4})^+$. The silicon atoms thus get a negative formal charge, Si^- . According to the Zintl-concept, a three-binding behavior is expected. This is realized by forming rows of six-membered rings in a boat configuration running in crystallographic b direction. Two of these rows are condensed in c direction. One third of the silicon atoms thus has only two silicon neighbors. The remaining bond is saturated by hydrogen atoms. The chemical formula can be reordered as $\text{Ca}^{2+}\text{H}^-[\text{Si}^-]_{2/3}[(\text{SiH})^-]_{1/3}$. The polyanion is a one-dimensional row of ${}^1[\text{HSi}_4\text{H}]^{4-}$ -units (Figure 1).

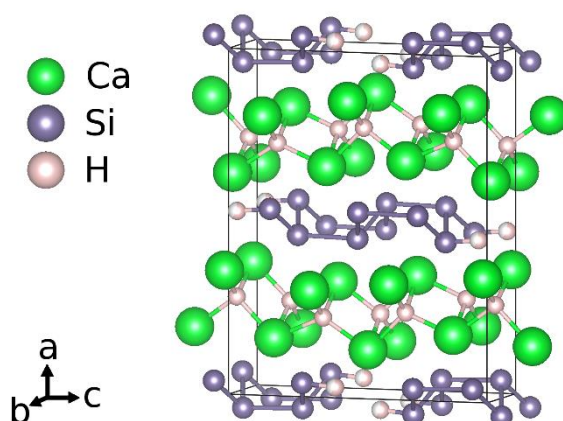


Figure 1. Crystal structure according to an idealized chemical formula $\text{CaSiH}_{4/3}$.

In addition to $\text{CaSiH}_{\approx 4/3}$, there are the isotopic compounds $\text{SrGeH}_{1.19}$, $\text{BaSnH}_{1.28}$ [18], and the structurally closely related compounds $\text{BaSiH}_{1.87}$ [18] as well as $\text{SrSiH}_{1.49}$ and $\text{BaGeH}_{1.56}$ [19,20], all of them showing a group 14 element-hydrogen contact. An intrinsic feature of these compounds is a pronounced under-occupation of the polyanion binding hydrogen site. For the title compound, this led to a controversy about the character of the bond.

Originally, a compound $\text{CaSiH}_{1.3}$ was described showing a short, covalent Si–H bond of 1.58 Å [17]. The structure was determined from X-ray powder diffraction and DFT calculations. All the silicon atoms are three binding (except for the non-stoichiometry of hydrogen) with almost equal Si–Si distances. A neutron diffraction and spectroscopy study were done on a deuterated compound $\text{CaSiD}_{1.2}$ [21]. This work describes a much longer Si–D distance of 1.82 Å. Further hydrogenation studies propose the composition $\text{CaSiH}_{1.06}$ [22]. The Rietveld analysis of the corresponding powder X-ray diffraction pattern confirms the heavy metal structure that was originally described. From ${}^2\text{H}$ solid state nuclear magnetic resonance spectroscopy we recently could estimate the Si–D bond length as 1.56(1) Å [23].

To end the controversy about chemical bonding in this compound, we combined a Rietveld analysis of X-ray and neutron powder diffraction patterns with small box pair distribution function (PDF) modelling of neutron total scattering data. Furthermore, we could identify new, hydrogen poor phases $\text{CaSiH}_{<1}$ by an in situ neutron diffraction study.

2. Results

The crystal structure of $\text{CaSiH}_{\approx 4/3}$ was reevaluated by a Rietveld analysis based on X-ray and neutron powder diffraction and a pair distribution function (PDF) analysis based on neutron total scattering data. The study considers a deuterated sample with a refined composition of $\text{CaSiD}_{1.1}$. Furthermore, the deuteration process was monitored in situ by neutron diffraction of a CaSi sample

under a deuterium gas atmosphere up to 5.5 MPa and elevated temperatures. At high temperatures (>520 K), hydrogen-poor phases $\text{CaSiD}_{x < 1}$ occur while the hydrogen-rich phase is formed upon cooling. Crystallographic information (CIF) for all phases can be found in the Supplementary Materials.

2.1. The Crystal Structure of $\text{CaSiD}_{1.1}$

The structural study of $\text{CaSiD}_{1.1}$ is based on a Zintl phase precursor that is almost phase pure (Figure 2). There is an impurity phase of CaO (2%) which is most probably introduced by the used calcium metal. There is a second impurity phase present that can hardly be seen in X-ray diffraction data (marked as * in Figure 2). Thus, the phases content appears neglectable. Both impurity phases do not change upon hydrogenation. Since the reflections of $\text{CaSiD}_{1.1}$ are strongly broadened, these two phases appear more pronounced in the diffraction pattern. We want to emphasize that the integrated intensity of the impurity phases is still negligible and does not influence the Rietveld or the PDF analysis.

2.1.1. Total Scattering and PDF Analysis

Fourier transforming properly corrected total scattering data leads to the pair distribution function (PDF; or, more general, the pair correlation function) of the atomic structure. Since it is a real-space representation of the structure, peaks can be directly interpreted as interatomic distances. A qualitative inspection of the neutron PDF data shows a first distance correlation at 1.53 Å. According to chemical reasoning, it can be directly assigned to the Si–D bond (Figure 3). The remaining atomic distance correlations need to be larger than 2 Å according to the crystal structure model which fits the PDF data.

Neutron PDF data were fitted using the crystallographic model in space group type $Pnma$ as shown in Figure 1. Atomic fractional coordinates were constrained according to the given symmetry. Modelling PDF data up to 30 Å results in a proper description of experimental data ($R_{\text{w,p}} = 0.165$; Figure 3). The refined Si1–D4 distance is 1.53 Å with an occupancy (SOF) of the D4 site of 0.35. Two of tetrahedral Ca_4 void are fully occupied. The corresponding SOF parameters were fixed during the last cycles. The D3 site is under-occupied as well (Table 1), giving a chemical formula $\text{CaSiD}_{1.08}$.

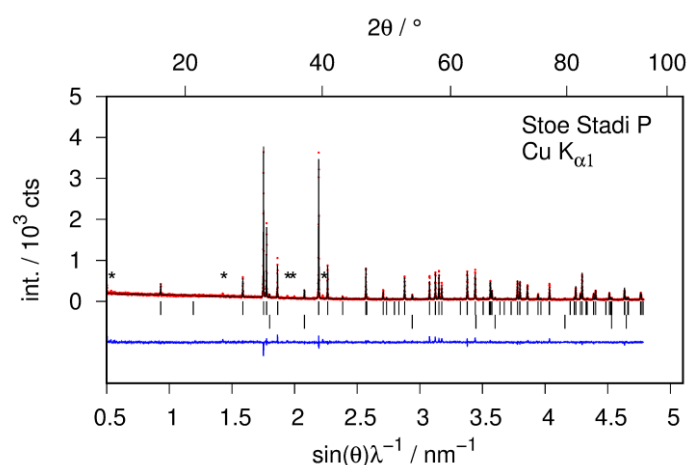


Figure 2. Quantitative phase analysis of the hydrogen-free sample CaSi by Rietveld analysis of X-ray powder diffraction data. Bragg marker: Top row CaSi (98 wt %); bottom row CaO (2 wt %). (*) marks minute intensities of an unidentified impurity phase; red points: observed intensity; black line: calculated intensity; blue line: difference plot.

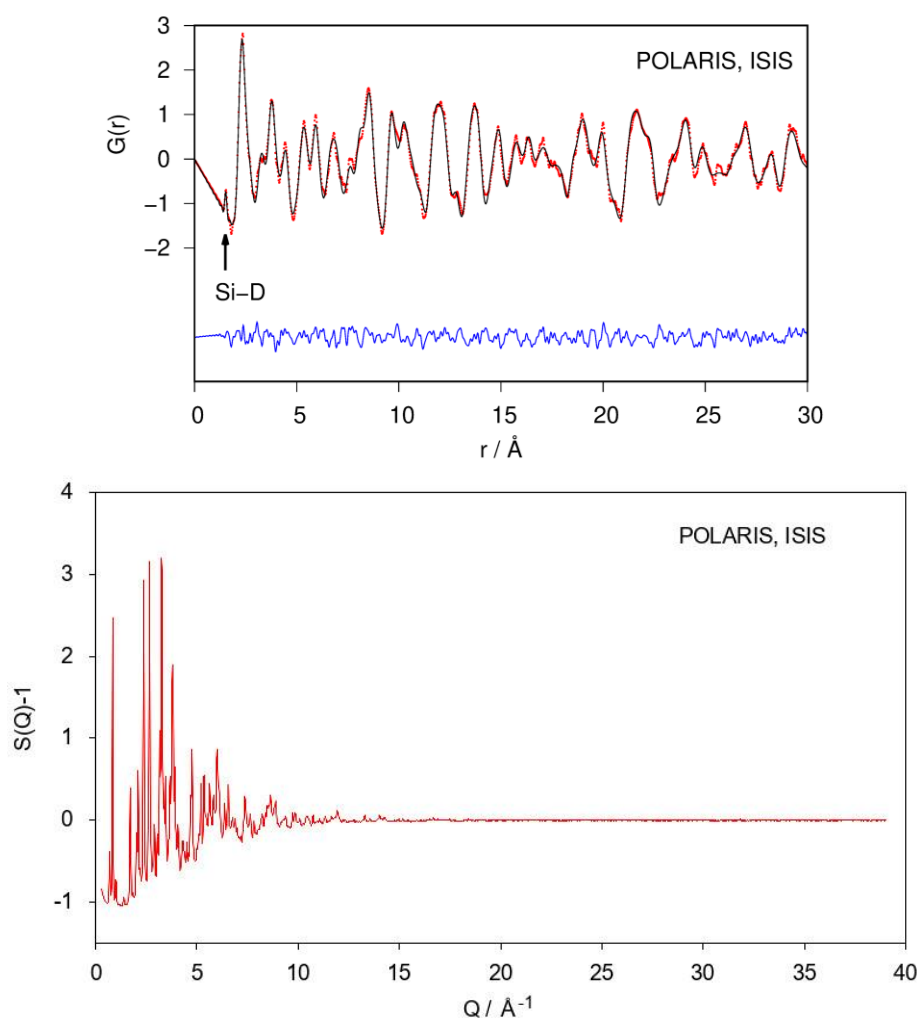


Figure 3. Refinement of the crystal structure of $\text{CaSiD}_{1.1}$ (space group $Pnma$) using neutron pair distribution function (PDF)-data (**top**) and corresponding $S(Q)$ (**bottom**). The Si–D correlation is marked. $R_{\text{wp}} = 0.165$. Red points, observed intensity; black line, calculated intensity; blue line, difference plot.

Table 1. Crystallographic data of $\text{CaSiD}_{1.1}$, according to a Rietveld refinement with a bond length restraint ($a = 14.579(4) \text{ \AA}$, $b = 3.8119(4) \text{ \AA}$, $c = 11.209(2) \text{ \AA}$) and PDF small-box modelling ($a = 14.594 \text{ \AA}$, $b = 3.8200 \text{ \AA}$, $c = 11.230 \text{ \AA}$). Lattice parameters of the corresponding hydride $\text{CaSiH}_{\approx 1.1}$ are $a = 14.6356(10) \text{ \AA}$, $b = 3.81207(15) \text{ \AA}$, $c = 11.2115(7) \text{ \AA}$, based on laboratory X-ray diffraction.

Atom	Rietveld					PDF				
	x	y	z	$B_{\text{iso}}/\text{\AA}^2$	SOF	x	y	z	$B_{\text{iso}}/\text{\AA}^2$	SOF
Ca1	0.3381(3)	$\frac{1}{4}$	0.8453(5)	1.07(18)	1	0.3412	$\frac{1}{4}$	0.8532	0.94	1
Ca2	0.3113(2)	$\frac{1}{4}$	0.1571(5)	$B_{\text{iso}}(\text{Ca1})$	1	0.3116	$\frac{1}{4}$	0.1522	0.94	1
Ca3	0.3592(2)	$\frac{1}{4}$	0.4810(4)	$B_{\text{iso}}(\text{Ca1})$	1	0.3633	$\frac{1}{4}$	0.4731	0.94	1
Si1	0.0436(5)	$\frac{1}{4}$	0.1795(5)	1.48(18)	1	0.0349	$\frac{1}{4}$	0.1795	1.03	1
Si2	0.0430(5)	$\frac{1}{4}$	0.7608(5)	$B_{\text{iso}}(\text{Si1})$	1	0.0430	$\frac{1}{4}$	0.7640	1.03	1
Si3	0.0417(4)	$\frac{1}{4}$	0.5270(6)	$B_{\text{iso}}(\text{Si1})$	1	0.0396	$\frac{1}{4}$	0.5373	1.03	1
D1	0.2508(9)	$\frac{1}{4}$	0.8265(13)	1.05(15)	1	0.2436	$\frac{1}{4}$	0.8408	1.26	1
D2	0.2227(9)	$\frac{1}{4}$	0.1748(13)	$B_{\text{iso}}(\text{D1})$	0.95(3)	0.2219	$\frac{1}{4}$	0.1699	1.26	1
D3	0.2739(11)	$\frac{1}{4}$	0.4808(15)	$B_{\text{iso}}(\text{D1})$	0.81(2)	0.2816	$\frac{1}{4}$	0.4853	1.26	0.89
D4	0.0333(18)	$\frac{1}{4}$	0.045(2)	$B_{\text{iso}}(\text{D1})$	0.468(15)	0.0429	$\frac{1}{4}$	0.0437	0.87	0.35

According to the refined model, Si–Si distances within the zigzag chain (crystallographic *b* direction) are 2.31 Å. The chain-connection bond (crystallographic *c* direction) is 2.55 Å long. The Ca–D distances within the Ca₄D-tetrahedra reach from 2.15 Å to 2.54 Å.

2.1.2. Bragg Diffraction and Rietveld Analysis

The structural model of CaSiD_{1.1} was refined using X-ray and neutron diffraction data simultaneously (Figure 4, Table 1). Furthermore, the structure of the hydride CaSiH_{~1.1} was refined using laboratory X-ray data (hydrogen positions fixed according to CaSiD_{1.1}; data not shown). All crystallographic data are available in the Supplementary Materials.

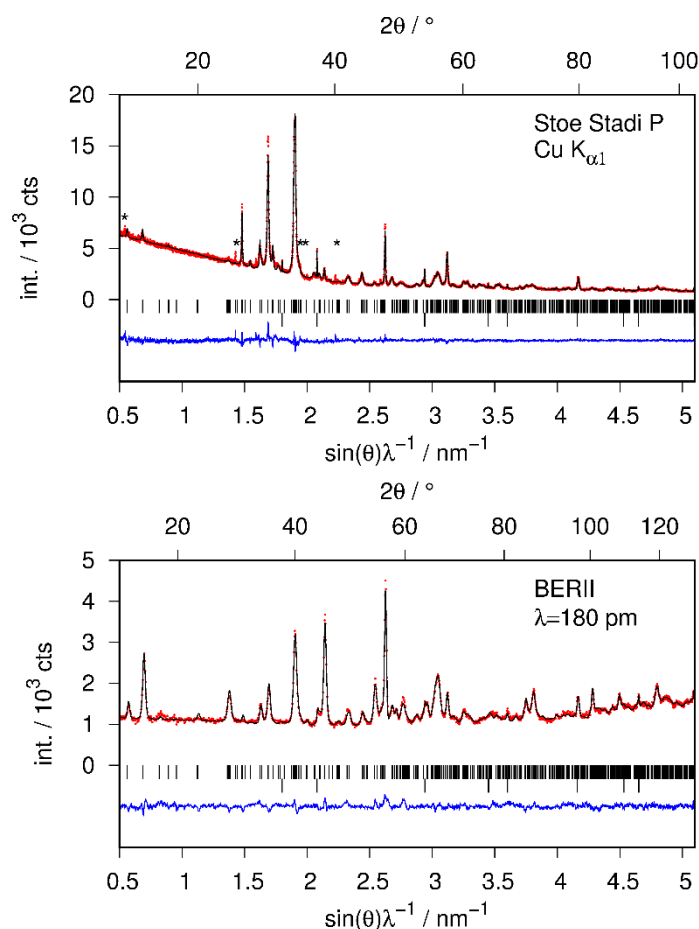


Figure 4. Rietveld of the crystal structure of CaSiD_{1.1} (*Pnma*) using X-ray (**top**) and neutron diffraction data (**bottom**) simultaneously; $R_{wp} = 4.20\%$, $R_p = 3.20\%$, $GoF = 1.90$; Bragg marker are: top row CaSiD_{1.1}, bottom row CaO (2 wt %); (*) marks an unidentified impurity phase already present in the pristine Zintl phase (see text); red points, observed intensity; black line, calculated intensity; blue line, difference plot.

The crystal structure refinements suffer from various complications. The reflection profiles are strongly broadened compared to the pristine Zintl phase. These effects are furthermore anisotropic. Reflections with a large *k*-component are much narrower than the remaining ones. This effect was treated by the empirical Stephens model [24] in Rietveld refinements, as implemented in TOPAS [25]. The anisotropic broadening effect can be sufficiently described by the two parameters *S*₄₀₀ and *S*₀₀₄ with a fixed profile mixing parameter of 1.0 (pure Lorentzian type) and might arise from anisotropic crystallite size broadening. A previous report states that the compound tends to delaminate perpendicular to

the crystallographic a axis as determined from SEM images [22]. Since the polyanions run along the crystallographic b direction, it appears reasonable that $(0k0)$ reflections are the sharpest ones.

The atomic parameters were refined with one Debye–Waller factor per atom type. Two of the tetrahedral Ca_4 voids are filled ($\text{SOF}(\text{D1}) = 1$ (fixed during the last cycle), $\text{SOF}(\text{D2}) = 0.95(3)$), which is in agreement with the PDF-model. The D3 site shows a lower occupancy of about 80%. A free refinement of the silicon-bound deuterium position leads to a short Si1–D4 bond smaller than 1.40 \AA , which is chemically unreasonable and contradicts total scattering data. The overall contribution of the D4 site to the diffraction pattern is quite small. Thus, a soft restraint was used to force the Si–D bond length to fit the PDF-derived value of 1.53 \AA . The effect of different restraint distances on the goodness of fit (GoF) is small, i.e., well below 1% (Figure 5). Since the effect on the overall profile fitting is small, and considering the PDF analysis, the usage of a bond-length restraint is justified.

The restraint crystallographic model gives a Si–D bond length of $1.52(3) \text{ \AA}$ in a Rietveld refinement (Figure 4). The occupancy of the D4 site is $0.468(15)$. The Si–Si distance within the chain is $2.382(6) \text{ \AA}$ long, while the chain connecting bond is $2.621(9) \text{ \AA}$. Within the Ca_4D -tetrahedra the Ca–D distances reach from $2.104(16)$ to $2.479(15) \text{ \AA}$.

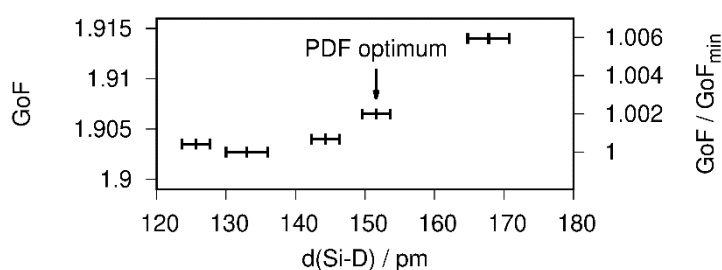


Figure 5. Influence of the Si–D bond length on the goodness of fit (GoF) of the Rietveld refinement of the crystal structure of $\text{CaSiD}_{1.1}$ (space group $Pnma$) based on neutron diffraction data.

2.2. In Situ Diffraction of the Hydrogenation Reaction and Hydrogen-Poor Phases

The hydrogenation of CaSi was monitored by in situ neutron powder diffraction. Heating the pristine Zintl phase to 520 K before pressurizing the in situ cell suppresses the formation of $\text{CaSiD}_{1.1}$. Instead, deuterium-poor phases $\text{CaSiD}_{<1}$ are formed. Fast heating under deuterium pressure leads to the same result. Deuterium uptake starting from the pristine phase takes about 10 min to finish. Subsequent dedeuteration (vacuum) and redeuteration (about 5 MPa D_2) cycles are very fast with less than 1 min until completion.

In a first step, CaSi reacted at 524 K and 5.5 MPa D_2 pressure (Table 2, (a)). Deuterium was released from the sample, reducing the gas pressure to 0.2 MPa (Table 2, (d)). In a second step, the sample was redeuterated at 3 MPa D_2 (Table 2, (b)), again dedeuterated at 0.2 MPa (Table 2, (e)), and finally under applied vacuum ($\approx 1 \text{ Pa}$, Table 2, (f)). In the end, the gas pressure was increased to 5.5 MPa again (Table 2, (c)), leading to the largest hydrogen incorporation.

Table 2. Deuterium-poor phases CaSiD_x , $x = \text{SOF}$. Labels refer to Figure 7.

Label	T/K	P/MPa	$a/\text{\AA}$	$b/\text{\AA}$	$c/\text{\AA}$	$\text{SOF}(\text{D})$	$d(\text{Si–Si})/\text{\AA}$
(a)	524	5.5	4.5206(7)	11.0166(14)	3.9018(5)	0.126(6) ^a	2.519(9)
(b)	535	3.0	4.5227(5)	11.0069(10)	3.9015(4)	0.137(5)	2.500(7)
(c)	537	5.5	4.5184(5)	11.0248(10)	3.9012(3)	0.168(6)	2.492(7)
(d)	529	0.2	4.5391(6)	10.9521(15)	3.9028(6)	0.092(5)	2.517(7)
(e)	537	0.2	4.5406(6)	10.9430(15)	3.9036(6)	0.096(6)	2.520(9)
(f)	537	$\approx 10^{-5}$	4.5607(6)	10.8469(12)	3.9039(5)	0.047(5)	2.514(6)

^a The first deuteration step shows a slow kinetic, thus, the maximal possible deuterium occupation might not be reached during the first step.

The hydrogen-poor phases $\text{CaSiD}_{<1}$ keep the structure of the pristine Zintl phase (Figure 6). Tetrahedral Ca_4 voids get partially filled. The occupation of the voids $\text{SOF} = x$ corresponds to the chemical formula CaSiD_x . Experimental conditions, compositions, and selected structural parameters can be found in Table 2. Rietveld profiles are given in Figure 7.

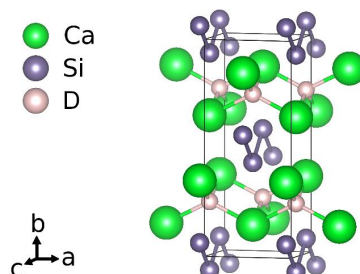


Figure 6. Crystal structure of the deuterium-poor phase CaSiD_x . The tetrahedral Ca_4 voids are partially filled. The $\text{SOF}(\text{D})$ corresponds to x in the chemical formula.

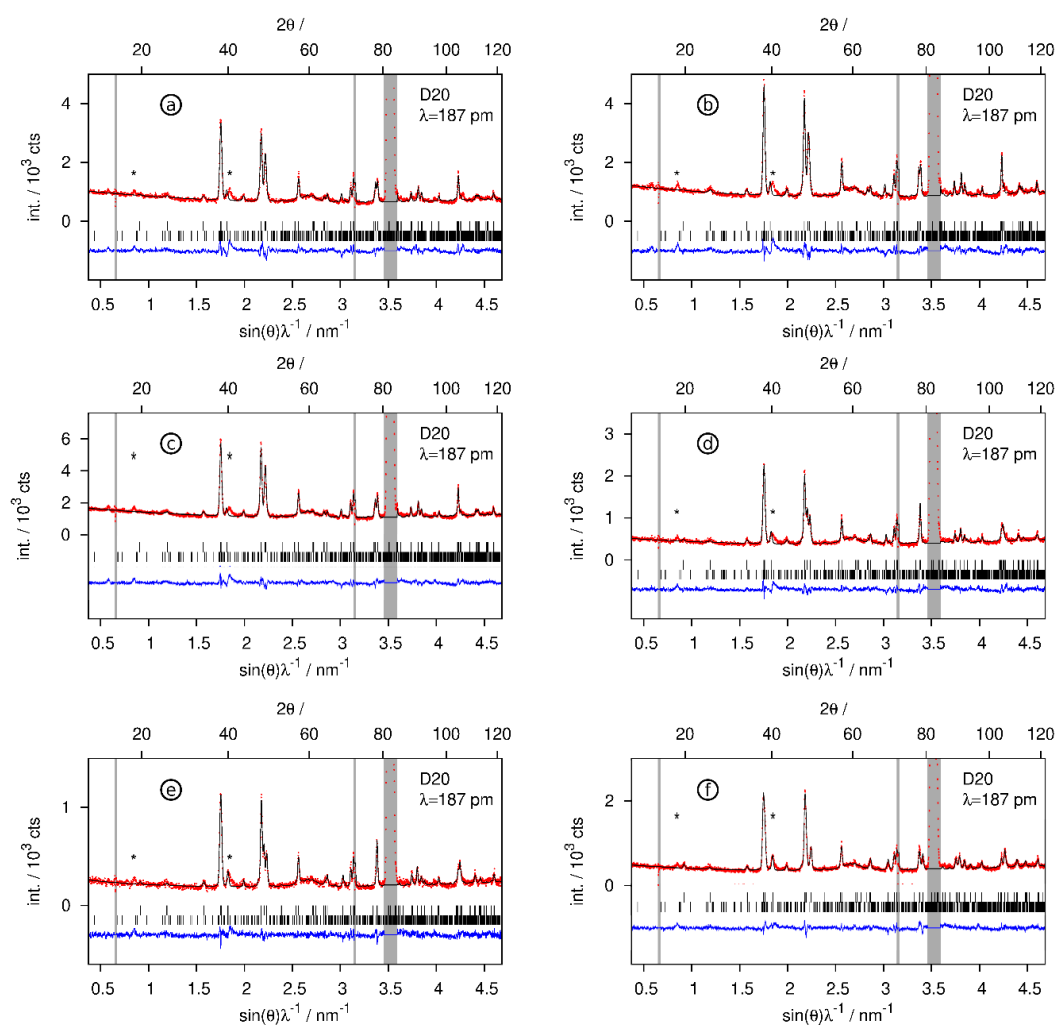


Figure 7. Rietveld refinements of the crystal structures of the deuterium-poor $\text{CaSiD}_{x<1}$ phases. Neutron diffraction data were collected in situ according to the conditions given in Table 2. The grey regions correspond to contributions of the sapphire cell. (*) marks unidentified peaks already present in the pristine Zintl phase. Bragg markers: CaSiD_x (top) and $\text{Ca}_{14}\text{Si}_{17}$ (bottom). (a) $\text{CaSiD}_{0.126(6)}$ (first deuteration cycle), (b) $\text{CaSiD}_{0.137(5)}$, (c) $\text{CaSiD}_{0.168(6)}$, (d) $\text{CaSiD}_{0.092(5)}$, (e) $\text{CaSiD}_{0.096(6)}$, (f) $\text{CaSiD}_{0.047(5)}$. Red points, observed intensity; black line, calculated intensity; blue line, difference plot.

3. Discussion

3.1. The Crystal Structure of $\text{CaSiD}_{1.1}$

The crystal structure of $\text{CaSiD}_{1.1}$ was determined by complementary techniques, i.e., a Rietveld and a PDF analysis. Both evaluations give a conclusive picture. The structural model originally described by Ohba et al. [17] can be confirmed. On the other hand, we do not find any indication of the presence of a phase that corresponds to the structure or the composition as described by Wu et al. [21]. The compound $\text{CaSiD}_{1.1}$ exhibits a polyanionic hydride moiety with a short Si–D distance of 1.53 Å. This is clearly in a covalent range and agrees well with a recent nuclear magnetic resonance study that estimates the bond length as 1.56(1) Å [23]. The silicon bound deuterium position is heavily under-occupied with only $35\% \leq \text{SOF} \leq 46\%$. There is a discrepancy between PDF and Rietveld analysis. The collection of total scattering data was done about one year after the Bragg diffraction study. The deuterium content of $\text{CaSiD}_{1.1}$ might be variable in a small range. We found such an indication also for a similar compound, $\text{SrGeD}_{1.2}$ [18]. Except for the SOF, the overall agreement between PDF and Rietveld analysis is considerable, as shown for the polyanion (Figure 8).

While tetrahedral voids are usually considered to be fully occupied by hydrogen atoms, we find a significant under-occupation of the D3 site. This position shows the shortest distance to the also under-occupied silicon bound D4 position. The SOF of the D2 and D1 site are not significantly different from unity (SOF(D1) was actually fixed during the last refinement cycles).

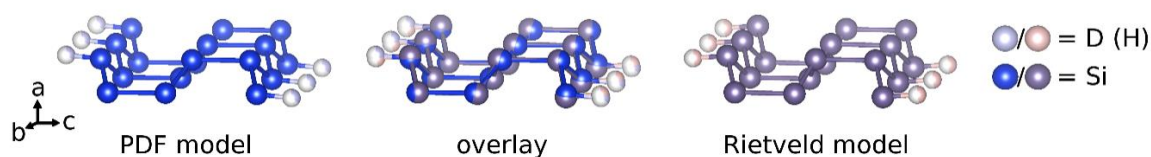


Figure 8. Comparison of the polyanionic structures as determined by the PDF and the Rietveld model (with constrained Si–D distance). The overlay of both models is shown in the middle.

3.2. Deuterium-Poor Phases

Hydrogen-poor phases $\text{CaSiD}_{x < 1}$ were identified in in situ experiments. These phases keep the structure of the pristine Zintl phase without any indication of deuterium ordering in the tetrahedral Ca_4 voids. They therefore can be compared to $\alpha\text{-BaGeD}_x$, $\alpha\text{-BaSnD}_x$ [26], and $\alpha\text{-SrGeD}_x$ [27], which all show a deuterium content $x < 0.5$. It was argued before that the formation of hydride/deuteride anions leads to a partial oxidation of the Si^{2-} zigzag chains. Since π^* bands get depopulated, the Si–Si bond length should decrease. Such a trend can indeed be seen (Table 2), but the effect is smaller than the estimated error.

Deuterium incorporation leads to an anisotropic expansion of the unit cell (Figure 9). The effect on lattice parameters is strongly anisotropic; a decreases, b expands, and c , which is the direction of the Si zigzag chains, is hardly affected. This is quite typical for the deuterium-poor phases [26,27].

The first deuterium uptake is a slow process. After an initial deuteration, compositional changes are very fast in regard to deuterium pressure changes. It is not possible to remove all of the deuterium from the structure. Similar results were found when desorption isotherms were determined [28].

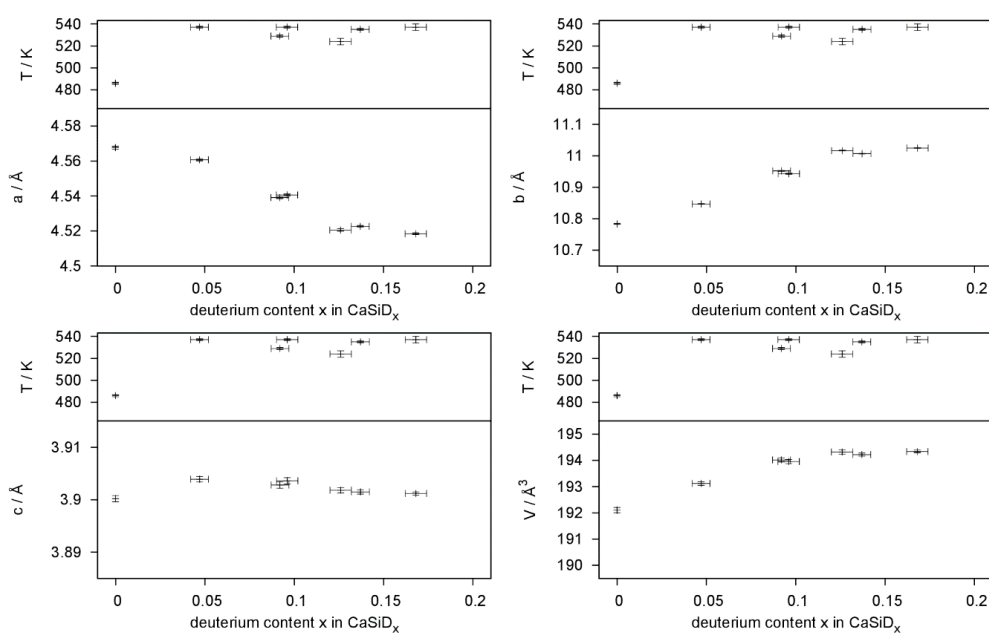


Figure 9. Change of lattice parameters and unit cell volume with respect to the deuterium incorporation.

4. Conclusions

The crystal structure of the Zintl phase hydride $\text{CaSiH}_{\approx 4/3}$ was controversial with regard to the nature of the interaction between silicon and hydrogen atoms. A combined neutron powder and total scattering study on the deuteride $\text{CaSiD}_{1.1}$ clearly shows a Si–D distance of 1.53 Å, which is in the range of typical covalent bonds. Therefore, a description with a limiting ionic formula $\text{Ca}^{2+}\text{H}(\text{Si}^-)_{2/3}(\text{SiH}^-)_{1/3}$ gives an appropriate description. It is emphasizing the main structural features, hydride anions in Ca_4 tetrahedra and silicon-hydrogen polyanions consisting of a ribbon-like polyanion made of three zigzag chains decorated by covalently bound hydrogen atoms. The latter position is under-occupied, thus resulting in a composition $\text{CaSiH}_{1.1}$. The crystal structure is isotypic to those of $\text{SrGeH}_{\approx 4/3}$ and $\text{BaSnH}_{\approx 4/3}$, and closely related to those of $\text{SrSiH}_{\approx 5/3}$, $\text{BaGeH}_{\approx 5/3}$, and $\text{BaSiH}_{\approx 2}$, which also show hydrogen decorated group 14 element polyanions.

In situ neutron powder diffraction showed that at 520 K deuterium-poor phases $\text{CaSiD}_{<1}$ form upon increasing the deuterium pressure instead of $\text{CaSiD}_{1.1}$. While the initial deuterium uptake starting from the pristine phase takes about 10 min to finish, subsequent cycles complete in less than 1 min. Such fast kinetics is beneficial for the potential use as hydrogen storage material. The crystal structure is that of the Zintl phase with hydride ions residing in tetrahedral Ca_4 voids with occupation $0.05 \leq x \leq 0.17$ in CaSiD_x , depending on temperature and deuterium pressure.

This study underlines the rich structural chemistry of Zintl phase hydrides. It further shows the limits of powder diffraction methods in cases where complications like pseudo-symmetry, anisotropic reflection broadening, high defect concentration, and the presence of light elements diminish the information content of diffraction data and the averaging character of diffraction methods blurs certain structural features. In such cases, methods like total scattering, nuclear magnetic resonance, and quantum-mechanical, calculations are indispensable for a complete picture of the crystal structure.

5. Materials and Methods

All educts and samples were handled in an argon filled glove box. Moisture and oxygen content were each kept below 1 ppm. Indeed, $\text{CaSiD}_{1.1}/\text{CaSiH}_{1.1}$ is stable in air over months and decomposes only slowly in water.

The Zintl phase CaSi was prepared from stoichiometric mixtures of the elements (Si: abcr, (Karlsruhe, Germany), 99.9999%; Ca: Alfa Aesar, (Kandel, Germany), 99.5%) using tantalum metal

jackets which were subsequently sealed and fused into silica ampoules at reduced pressure. They were heated with $2.2 \text{ K}\cdot\text{min}^{-1}$ to 1573 K and kept there for one hour. The samples then were annealed at 1473 K for 12 h. According to the literature, the CaSi containing ampoules need to be fast-quenched in cold water to obtain samples reactive towards hydrogen [14,22,29]. We want to emphasize that this step is a crucial one.

The deuterides were prepared in a Nicrofer 5219Nb-alloy 718 autoclave (home built) at deuterium gas pressures of 15 MPa and 523 K. The samples were annealed for 72 h.

X-ray diffraction was done on a laboratory Stadi P diffractometer (STOE & Cie, Darmstadt, Germany). The instrument is equipped with a sealed copper X-ray tube and a germanium monochromator (Cu $K\alpha_1$ radiation). Data were collected with a position sensitive Mythen 1K silicon-strip detector. Measurements were done in Debye-Scherrer geometry using 0.2 mm glass capillaries.

Neutron powder diffraction was performed at the E9 FIREPOD diffractometer [30] at the reactor source BERII of the Helmholtz-Zentrum Berlin (HZB), Germany on samples enclosed in 6 mm vanadium cans at a constant wave length of 1.7982 \AA .

In situ neutron diffraction of the deuteration process was performed at the D20 instrument [31] at the reactor source of the Institut-Laue-Langevin (ILL), Grenoble, France. The experiments were done in home-build sapphire single-crystal cells attached to a gas supply system. Heating was realised by two infrared laser beams. Details of the setup were already described elsewhere [32,33]. Measurements were done at a constant wavelength of 1.86829 \AA .

Powder diffraction data were treated by the Rietveld method [34,35] as implemented in the program Topas [25].

Neutron total scattering experiments were done at the time-of-flight (TOF) instrument POLARIS [36,37] of ISIS spallation source, Didcot, UK, on samples enclosed in 8 mm vanadium cans. Data and Proposal information can be accessed under reference [38]. Data reduction was done using the GunrunN package [39]. Data were corrected for background using measurements of an empty vanadium can and the empty instrument. To get an absolute data scale, intensities were normalized to the measurement of a vanadium rod with 5 mm diameter. The maximum of reciprocal space data used for the Fourier transformation was set to 39 \AA^{-1} . The minimum real space radius for the Fourier transform was set to 1.15 \AA .

The obtained real space pair distribution function was evaluated using small box modelling. A crystallographic model (full symmetry) was fitted to the data using pdfGUI [40].

All graphs were prepared using the program Gnuplot [41]. Molecular and crystal structures were prepared using VESTA [42,43].

Supplementary Materials: The following are available online at <http://www.mdpi.com/2304-6740/7/9/106/s1>; CIF and checkCIF output files for the following compounds with file names compound datasource (COD-number; CSD-number). CaSiH_x_stoe.cif (3000246; 1918684), CaSiD_{0.047}_ILL.cif (3000247; 1918677), CaSiD_{0.092}_ILL.cif (3000248; 1918678), CaSiD_{0.096}_ILL.cif (3000249; 1918679), CaSiD_{0.126}_ILL.cif (3000250; 1918680), CaSiD_{0.137}_ILL.cif (3000251; 1918681), CaSiD_{0.168}_ILL.cif (3000252; 1918682), CaSiD_{1.2}_BERII.cif (3000253; 1918683). CIFs may also be obtained from the Fachinformationszentrum Karlsruhe, 76344 Eggenstein-Leopoldshafen, Germany (Fax: +49-7247-808-666; E-Mail: crysdata@fiz-karlsruhe.de, <http://www.fiz-karlsruhe.de/requestfordepositeddata.html>) on quoting the depository numbers CSD-1918677 (CaSiD_{0.047}), CSD-1918678 (CaSiD_{0.092}), CSD-1918679 (CaSiD_{0.096}), CSD-1918680 (CaSiD_{0.126}), CSD-1918681 (CaSiD_{0.137}), CSD-1918682 (CaSiD_{0.168}), CSD-1918683 (CaSiD_{1.1}) and CSD-1918684 (CaSiH_{1.1}); The crystallographic data are also available free of charge at the Crystallographic Open Database (COD) under the following deposition numbers: 3000247 (CaSiD_{0.047}), 3000248 (CaSiD_{0.092}), 3000249 (CaSiD_{0.096}), 3000250 (CaSiD_{0.126}), 3000251 (CaSiD_{0.137}), 3000252 (CaSiD_{0.168}), 3000253 (CaSiD_{1.1}) and 3000246 (CaSiH_{1.1}).

Author Contributions: Conceptualization, H.A. and H.K.; methodology, H.A.; validation, H.A. and F.Y.; formal analysis, H.A.; investigation, H.A., F.Y., H.Y.P., A.F. and T.C.H.; writing—original draft preparation, H.A. and F.Y.; writing—review and editing, all authors; visualization, H.A.; supervision, H.K.; funding acquisition, H.K. and H.A.

Funding: This research was funded by DEUTSCHE FORSCHUNGSGEMEINSCHAFT (DFG), grant number KO1803/7 and FONDS DER CHEMISCHEN INDUSTRIE, grant number 194371.

Acknowledgments: We thank Helmholtz-Zentrum Berlin (Berlin, Germany), Institut Laue-Langevin (Grenoble, France) and The ISIS Facility (Didcot, UK) for the allocation of neutron radiation beamtime.

Conflicts of Interest: The authors declare no conflict of interest. The funders had no role in the design of the study; in the collection, analyses, or interpretation of data; in the writing of the manuscript, or in the decision to publish the results.

References

1. Gingl, F.; Vogt, T.; Akiba, E. Trigonal SrAl₂H₂: the first Zintl phase hydride. *J. Alloys Compd.* **2000**, *306*, 127–132. [[CrossRef](#)]
2. Björling, T.; Noréus, D.; Häussermann, U. Polyanionic Hydrides from Polar Intermetallics AeE₂ (Ae = Ca, Sr, Ba; E = Al, Ga, In). *J. Am. Chem. Soc.* **2006**, *128*, 817–824. [[CrossRef](#)]
3. Lee, M.H.; Björling, T.; Hauback, B.C.; Utsumi, T.; Moser, D.; Bull, D.; Noréus, D.; Sankey, O.F.; Häussermann, U. Crystal structure, electronic structure, and vibrational properties of MAISiH (M = Ca, Sr, Ba): Hydrogenation-induced semiconductors from the AlB₂-type alloys MAISi. *Phys. Rev. B* **2008**, *78*, 195209. [[CrossRef](#)]
4. Lee, M.H.; Evans, M.J.; Daemen, L.L.; Sankey, O.F.; Häussermann, U. Vibrational Property Study of SrGa₂H₂ and BaGa₂H₂ by Inelastic Neutron Scattering and First Principles Calculations. *Inorg. Chem.* **2008**, *47*, 1496–1501. [[CrossRef](#)]
5. Evans, M.J.; Holland, G.P.; Garcia-Garcia, F.J.; Häussermann, U. Polyanionic Gallium Hydrides from AlB₂-Type Precursors AeGaE (Ae = Ca, Sr, Ba; E = Si, Ge, Sn). *J. Am. Chem. Soc.* **2008**, *130*, 12139–12147. [[CrossRef](#)] [[PubMed](#)]
6. Kranak, V.F.; Evans, M.J.; Daemen, L.L.; Proffen, T.; Lee, M.H.; Sankey, O.F.; Häussermann, U. Structural and dynamic properties of the polyanionic hydrides SrAlGeH and BaAlGeH. *Solid State Sci.* **2009**, *11*, 1847–1853. [[CrossRef](#)]
7. Evans, M.J.; Kranak, V.F.; Garcia-Garcia, F.J.; Holland, G.P.; Daemen, L.L.; Proffen, T.; Lee, M.H.; Sankey, O.F.; Häussermann, U. Structural and Dynamic Properties of BaInGeH: A Rare Solid-State Indium Hydride. *Inorg. Chem.* **2009**, *48*, 5602–5604. [[CrossRef](#)]
8. Evans, M.J.; Lee, M.H.; Holland, G.P.; Daemen, L.L.; Sankey, O.F.; Häussermann, U. Vibrational properties of the gallium monohydrides SrGaGeH, BaGaSiH, BaGaGeH, and BaGaSnH. *J. Solid State Chem.* **2009**, *182*, 2068–2073. [[CrossRef](#)]
9. Häussermann, U.; Kranak, V.F.; Puhakainen, K. Hydrogenous Zintl Phases: Interstitial Versus Polyanionic Hydrides. *Struct. Bond.* **2010**, *139*, 143–161. [[CrossRef](#)]
10. Ångström, J.; Johansson, R.; Sarkar, T.; Sørby, M.H.; Zlotea, C.; Andersson, M.S.; Nordblad, P.; Scheicher, R.H.; Häussermann, U.; Sahlberg, M. Hydrogenation-Induced Structure and Property Changes in the Rare-Earth Metal Gallide NdGa: Evolution of a [GaH]²⁻ Polyanion Containing Peierls-like Ga–H Chains. *Inorg. Chem.* **2016**, *55*, 345–352. [[CrossRef](#)]
11. Auer, H.; Nedumkandathil, R.; Häussermann, U.; Kohlmann, H. The Hydrogenation of the Zintl Phase NdGa Studied by in situ Neutron Diffraction. *Z. Anorg. Allg. Chem.* **2019**, *645*, 175–181. [[CrossRef](#)]
12. Nedumkandathil, R.; Kranak, V.F.; Johansson, R.; Ångström, J.; Balmes, O.; Andersson, M.S.; Nordblad, P.; Scheicher, R.H.; Sahlberg, M.; Häussermann, U. Hydrogenation Induced Structure and Property Changes in GdGa. *J. Solid State Chem.* **2016**, *239*, 184–191. [[CrossRef](#)]
13. Werwein, A.; Benndorf, C.; Bertmer, M.; Franz, A.; Oeckler, O.; Kohlmann, H. Hydrogenation Properties of LnAl₂ (Ln = La, Eu, Yb), LaGa₂, LaSi₂ and the Crystal Structure of LaGa₂H_{0.71(2)}. *Crystals* **2019**, *9*, 193. [[CrossRef](#)]
14. Aoki, M.; Ohba, N.; Noritake, T.; Towata, S. Reversible hydriding and dehydriding properties of CaSi: Potential of metal silicides for hydrogen storage. *Appl. Phys. Lett.* **2004**, *85*, 387–388. [[CrossRef](#)]
15. Ohba, N.; Aoki, M.; Noritake, T.; Miwa, K.; Towata, S.-i. Development of New Hydrogen Storage Material CaSi Theoretical Prediction and Experiment. *RD Rev. Toyota CRDL* **2004**, *39*, 40–45.
16. Aoki, M.; Ohba, N.; Noritake, T.; Towata, S.-i. Hydriding and dehydriding properties of CaSi. *J. Alloys Compd.* **2005**, *404*, 402–404. [[CrossRef](#)]
17. Ohba, N.; Aoki, M.; Noritake, T.; Miwa, K.; Towata, S.-i. First-principles study of a hydrogen storage material CaSi. *Phys. Rev. B* **2005**, *72*, 075104. [[CrossRef](#)]

18. Auer, H.; Guehne, R.; Bertmer, M.; Weber, S.; Wenderoth, P.; Hansen, T.C.; Haase, J.; Kohlmann, H. Hydrides of Alkaline Earth-Tetrel (*AeTt*) Zintl Phases: Covalent *Tt*-H Bonds from Silicon to Tin. *Inorg. Chem.* **2017**, *56*, 1061–1071. [CrossRef]
19. Auer, H.; Schlegel, R.; Oeckler, O.; Kohlmann, H. Structural and Electronic Flexibility in Hydrides of Zintl Phases with Tetrel-Hydrogen and Tetrel-Tetrel Bonds. *Angew. Chem. Int. Ed.* **2017**, *56*, 12344–12347. [CrossRef]
20. Auer, H.; Schlegel, R.; Oeckler, O.; Kohlmann, H. Strukturelle und elektronische Flexibilität in Hydriden von Zintl-Phasen mit Tetrel-Wasserstoff- und Tetrel-Tetrel-Bindung. *Angew. Chem.* **2017**, *129*, 12515–12518. [CrossRef]
21. Wu, H.; Zhou, W.; Udovic, T.J.; Rush, J.J.; Yildirim, T. Structure and hydrogen bonding in CaSiD_{1+x} Issues about covalent bonding. *Phys. Rev. B* **2006**, *74*, 224101. [CrossRef]
22. Armbruster, M.; Wörle, M.; Krumeich, F.; Nesper, R. Structure and Properties of Hydrogenated Ca, Sr, Ba, and Eu Silicides. *Z. Anorg. Allg. Chem.* **2009**, *635*, 1758–1766. [CrossRef]
23. Guehne, R.; Auer, H.; Kohlmann, H.; Haase, J.; Bertmer, M. Determination of element-deuterium bond lengths in Zintl phase deuterides by 2H-NMR. *Phys. Chem. Chem. Phys.* **2019**, *21*, 10594–10602. [CrossRef] [PubMed]
24. Stephens, P.W. Phenomenological model of anisotropic peak broadening in powder diffraction. *J. Appl. Crystallogr.* **1999**, *32*, 281–289. [CrossRef]
25. Bruker AXS. TOPAS Version 5. Available online: www.bruker-axs.com (accessed on 25 June 2019).
26. Auer, H.; Weber, S.; Hansen, T.C.; Többens, D.M.; Kohlmann, H. Reversible hydrogenation of the Zintl phases BaGe and BaSn studied by in situ diffraction. *Z. Kristallogr. Cryst. Mater.* **2018**, *233*, 399–409. [CrossRef]
27. Auer, H.; Wallacher, D.; Hansen, T.C.; Kohlmann, H. In Situ Hydrogenation of the Zintl Phase SrGe. *Inorg. Chem.* **2017**, *56*, 1072–1079. [CrossRef] [PubMed]
28. Anikina, E.Y.; Verbetsky, V.N. Investigation of hydrogen desorption from CaSiH by means of calorimetric method. *J. Therm. Anal. Calorim.* **2014**, *118*, 801–805. [CrossRef]
29. Wenderoth, P. Untersuchungen zur Hydridbildung von Zintl-Phasen der Erdalkalimetalle mit Aluminium, Gallium und Silicium. Ph.D. Thesis, Universität des Saarlandes, Saarbrücken, Germany, 2014.
30. Franz, A.; Hoser, A. E9: The Fine Resolution Powder Diffractometer (FIREPOD) at BER II. *J. Large-Scale Res. Facil.* **2017**, *3*, A103. [CrossRef]
31. Hansen, T.C.; Henry, P.F.; Fischer, H.E.; Torregrossa, J.; Convert, P. The D20 instrument at the ILL: A versatile high-intensity two-axis neutron diffractometer. *Meas. Sci. Technol.* **2008**, *19*, 034001. [CrossRef]
32. Kohlmann, H.; Kurtzemann, N.; Wehrich, R.; Hansen, T. In situ Neutron Powder Diffraction on Intermediate Hydrides of MgPd_3 in a Novel Sapphire Gas Pressure Cell. *Z. Anorg. Allg. Chem.* **2009**, *635*, 2399–2405. [CrossRef]
33. Götze, A.; Auer, H.; Finger, R.; Hansen, T.; Kohlmann, H. A sapphire single-crystal cell for in situ neutron powder diffraction of solid-gas reactions. *Phys. B* **2018**, *551*, 395–400. [CrossRef]
34. Rietveld, H.M. Line profiles of neutron powder-diffraction peaks for structure refinement. *Acta Crystallogr.* **1967**, *22*, 151–152. [CrossRef]
35. Rietveld, H.M. A profile refinement method for nuclear and magnetic structures. *J. Appl. Crystallogr.* **1969**, *2*, 65–71. [CrossRef]
36. Hull, S.; Smith, R.I.; David, W.I.F.; Hannon, A.C.; Mayers, J.; Cywinski, R. The Polaris powder diffractometer at ISIS. *Phys. B* **1992**, *180*, 1000–1002. [CrossRef]
37. Smith, R.I.; Hull, S.; Tucker, M.; Playford, H.Y.; McPhail, D.; Waller, S.; Norberg, S. The Upgraded Polaris Powder Diffractometer at ISIS. *Rev. Sci. Inst.* **2019**. submitted for publication.
38. Kohlmann, H.; Auer, H.; Playford, H.Y. Total scattering of Zintl phase deuterides $\text{CaSiD}_{1.3}$, $\text{BaSiD}_{1.9}$ and $\text{SrGeD}_{1.3}$. *STFC ISIS Neutron Muon Source* **2018**. [CrossRef]
39. Soper, A.K. *GudrunN and GudrunX programs for correcting raw neutron and X-ray diffraction data to differential scattering cross section*, RAL Technical Report; Science and Technology Facilities Council: Oxford, UK, 2011.
40. Farrow, C.L.; Juhas, P.; Liu, J.W.; Bryndin, D.; Bozin, E.S.; Bloch, J.; Proffen, T.; Billinge, S.J.L. PDFfit2 and PDFgui: computer programs for studying nanostructure in crystals. *J. Phys. Condens. Matter* **2007**, *19*, 335219. [CrossRef] [PubMed]
41. GNU PLOT Version 5.0, Patchlevel 7. Available online: <http://www.gnuplot.info> (accessed on 25 June 2019).

42. VESTA—Visualisation for Electronic and Structural Analysis. Version 3.3.1. Koichi Momma and Fujio Izumi: Ibaraki, Japan, 2018.
43. Momma, K.; Izumi, F. VESTA3 for three-dimensional visualization of crystal, volumetric and morphology data. *J. Appl. Crystallogr.* **2011**, *44*, 1272–1276. [[CrossRef](#)]



© 2019 by the authors. Licensee MDPI, Basel, Switzerland. This article is an open access article distributed under the terms and conditions of the Creative Commons Attribution (CC BY) license (<http://creativecommons.org/licenses/by/4.0/>).